Northumbria Research Link

Northumbria University
NEWCASTLE

UniversityLibrary

Ring-Core-Fibre Based Mode Division Multiplexing Systems

Jie Liu, Guoxuan Zhu, Junwei Zhang, Yuanhui Wen, Xiong Wu, Yanfeng Zhang, Yujie Chen, Xinlun Cai, Zhaohui Li, Ziyang Hu, Jiangbo Zhu, and Siyuan Yu

Abstract — **The unique modal characteristics of ring core fibres potentially enable the implementation of mode-division multiplexing (MDM) schemes that can increase optical data transmission capacity with either low complexity modular multi-input multi-output (MIMO) equalization or no MIMO. This paper attempts to present an comprehensive review of recent research on key aspects of RCF-based MDM transmission. Starting from fundamental fibre modal structures, a theoretical comparison between RCF and conventional step-index and graded-index multi-mode fibres in terms of their MDM capacity and the associated MIMO complexity is given first as the underlining rationale behind RCF-MDM. This is followed by a discussion of RCF design considerations for achieving high mode channel count and low crosstalk performances in either MIMO-free or modular MIMO transmission schemes. The principles and implementations of RCF mode (de-)multiplexing devices are discussed in detail, followed by RCF-based optical amplifiers, culminating in MIMO-free or modular MIMO RCF-MDM data transmission schemes. A discussion on further research directions is also given.**

Index Terms—**Ring-core fibre, mode-division multiplexing, Optical communications.**

I. INTRODUCTION

As conventional single mode fibre (SMF) starts to encounter major barriers to further increase in its information transmission capacity, a plurality of multiplexing schemes that explore the increased degree of freedom afforded in the transverse spatial domain of the optical fibre have been intensively studied over the last decade, aiming to sustain the necessary growth of optical fibre communication capacity that underpins the exponential growth of internet traffic [1, 2]. This expansion is possible because in the SMF, its 9-um diameter core area only occupies about 0.5% of the 125-um diameter fibre cross-sectional area - a very low utility of space. These new multiplexing schemes are often collectively known as spatial division multiplexing (SDM), which includes mode-division multiplexing (MDM) schemes using multimode fibres (MMFs) or few-mode fibres (FMFs) and/or core-multiplexing schemes using multicore fibres (MCFs) [1]. Compared to SDM schemes using spatially separate channels (cores), MDM

schemes using mode channels that overlap in a larger guiding core can be seen as an extreme case where the multiple single mode cores of an MCF merge to form a multi-mode core, which may provide higher capacity density (bit/s per unit cross-sectional area) and more compact inline devices (e.g. optical amplifiers). While the compactness of MDM could make the scaling of optical networks more cost effective and energy efficient [3-5], it however brings its own set of challenges.

Much research on MDM has been carried out on multi-mode or few-mode fibres (MMF or FMF) with the conventional step-index (SI) or graded-index (GI) structures. A main limitation to the effort to increase MDM capacity by using more mode channels is the sharply-increasing MIMO complexity, which in the transverse spatial dimension is roughly proportional to the square of the number of coupling modes, and in the time (or longitudinal) dimension proportional to the differential mode delay (DMD) between these modes. The rapidly-increasing MIMO complexity will eventually become prohibitively costly and power-hungry [6].

In order to improve the capacity of MDM systems without significantly increasing the MIMO-equalization complexity, many schemes have been proposed for both the long-haul and short-reach transmissions.

In long-haul MDM systems, coupling between all mode pairs is non-negligible [7]. Although strong modal coupling is shown to compress the impulse response and therefore suppress the DMD-related MIMO complexity [8], the transverse spatial dimension of the MIMO complexity remains difficult to address.

In short-reach MDM systems, within length scale of tens of kilometres (e.g. the metro, access, intra- or inter-data-center links, etc.), weak coupling may be maintained between modes or mode groups (MGs) with differential effective refractive index (Δn_{eff}) of $\sim 10^{-4}$ - 10^{-3} [9], potentially enabling partial-MIMO or MIMO-free schemes that improve system capacity with MIMO complexity [10-19]. In [10-12], weakly-coupled FMF transmission incorporating partial-MIMO processing is proposed, in which low inter-mode or inter-MG coupling is ensured by increasing Δn_{eff}, so that only smaller MIMO blocks are required to handle the polarization diversity and mode

degeneracy. However, the low MIMO complexity of such schemes may not be sustainable when higher order modes/MGs are explored, as the number of intra-MG modes increases with the mode/MG order. A MIMO-less approach has also been proposed using an elliptical-core FMF to further eliminate the mode degeneracy [13-15]. However, higher ellipticity may cut off the highest-order modes, resulting in a trade-off between the number of guided modes (capacity) and the achievable birefringence (DSP complexity) [16]. Elliptical fibres are also not friendly to conventional fibre making technologies. Mode group multiplexing (MGM) is another MIMO-free MDM transmission scheme, in which multiple (near-)degenerate modes within each MG of a GI-MMF are regarded as one data channel. By exploiting weak-coupling among different MGs, MIMO processing can be eliminated [17-20]. However, as the number of modes in each MG increases with the MG order, reception of high-order MGs will become more complicated, since all the intra-group modes need to be detected simultaneously at the receiver in the MGM scheme to avoid mode partition noise [19, 20].

Above problems associated with conventional MMF/FMF with step-index (SI) or graded-index (GI) refractive-index (RI) profiles has prompted the exploration of new types of fibres, which brings us to the subject matter of this paper, namely the ring core fibres (RCF).

Although the RCF was first proposed in the 1970s [21], it remained relatively obscure until very recently, when its potential as an alternative approach for achieving low-complexity and high-capacity MDM transmission has prompted a sharp rise in research activity.

As will be detailed, RCFs can limit the radial mode index to 1 and thereby fixing the number of modes in each high-order MG (MG order > 0) to 4, which would decrease the MIMO complexity and simplify the implementation of the high-order MG reception. Coupling between adjacent RCF MGs reduces as their azimuthal mode order increases [22], which could make RCFs more scalable towards the higher order mode space. In addition, RCF-based amplifiers can also provide more equalized gain for all guided signal modes because they have similar mode profiles [23, 24], which can reduce the differential modal gain (DMG). These characteristics make RCF-based MDM systems highly attractive.

In this paper, we review recent progress in RCF-based MDM research. The remainder of this paper is organized as follows. In Section II, a theoretical comparison is made between RCF-based MDM scheme and other MMF/FMF based MDM schemes in terms of system capacity (or spectral efficiency, SE) and MIMO complexity. This will be followed by a discussion on RCF characteristics and design in Section III. Section IV summarizes the reported optical mode multiplexer / demultiplexer technologies for RCFs. RCF-based optical amplifiers are reviewed in Section V. Section VI reviews the reported demonstrations of data transmission over RCF-based MDM systems. We conclude the paper with a discussion on future outlook in Section VII.

II. A THEORETICAL COMPARISON BETWEEN RCF AND MMF BASED MDM SYSTEMS

Although RCF-MDM schemes intuitively support better trade-off between the capacity or SE and the MIMO complexity, nevertheless a first-principle based quantitative comparison between RCF and conventional SI- and GI-MMF/FMF is needed to place this intuition on a solid ground, which is given in this section.

The comparison here is for short-reach transmission scenarios where weak modal coupling over the transmission link length can be ensured if the Δn_{eff} between the mode- or MG-pair involved is sufficiently large. Three kinds of optical fibres are considered, namely SI-MMF, GI-MMF, and SI-RCF with single radial mode. In the following, we firstly present the fibre RI parameters and modal coupling characteristics utilized in our calculations. These will be followed by the description of the communication channel and MIMO-equalizer model used for SE and complexity calculations, respectively. The calculation results are analysed to highlight the difference between MDM implemented over the three kinds of fibres. At last, challenges for practical implementations of RCF-based MDM systems are also pointed out.

A. Fibre Refractive-Index Profiles and Modal Coupling Characteristics

For all three kinds of fibres, we assume the maximum fibre core RI n_1=1.48 and the cladding RI n_2=1.45, a ~2% difference. The fibre material chromatic dispersion (CD) is ignored as it doesn't affect SE calculation. As an example, the RI profile for the conventional SI-MMF at 20-µm fibre core radius is shown in Fig.1(a). Under the weakly guiding condition [25], the number of supported modes M in a SI-MMF equals to $V^2/2$, where the normalized frequency of the fibre $V = k_0 a\sqrt{n_1^2 - n_2^2}$ with the core radius of R [26], and k_0 is the vacuum wave vector

The coupling coefficient between fibre modes can be quantified as [22, 27]

$$2\gamma_{nm} = k_0^2 \sqrt{\pi}\sigma^2 L_c \frac{4\kappa^2}{4\kappa^2 + \Delta\beta^2} \frac{\left[\int_0^b r \frac{\partial n}{\partial r} A_n A_m dr\right]^2}{\int_0^b |A_n|^2 rdr \int_0^b |A_m|^2 rdr} \quad (1)$$

where b is the cladding boundary radius, σ is the standard deviation of fibre perturbation and $L_c = \kappa^{-1}$ its correlation length. Both σ and L_c are highly dependent on imperfections in the fibre such as core-cladding boundary roughness and micro-bending. $\Delta\beta = 2\pi\Delta n_{eff}/\lambda$ is the propagation constant difference between the coupling modes n and m. A_n and A_m are normalized amplitude of modes n and m, respectively.
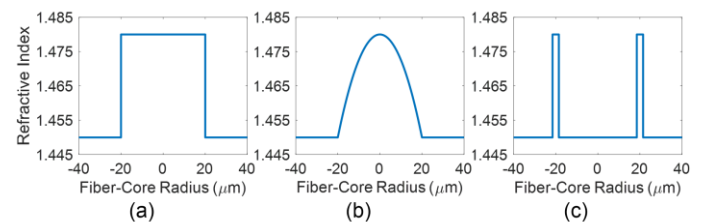

(a)   (b)   (c)

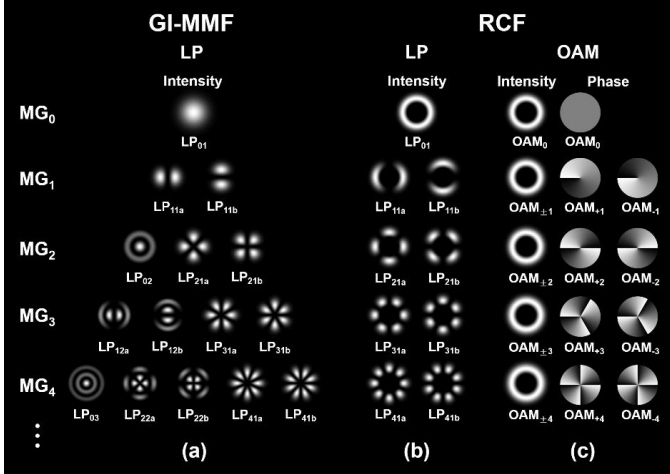Fig. 1. Refractive-index profiles of the (a) SI MMF; (b) GI MMF; (c) RCF at fibre-core radius of 20 µm.

Fig. 2. LP modes categorized in different MGs of the (a) GI-MMF and (b) RCF; (c) OAM modes categorized in different MGs of the RCF [28]. Here note that each fibre mode shown in this figure further has two orthogonal polarization states.

In the conventional SI-MMF, crosstalk between all adjacent linear polarized (LP) mode-pairs may be non-negligible because Δn_{eff} values tend to be similar between consecutive LP modes. For larger V, Δn_{eff} becomes small which results in relatively strong coupling between all modes as energy from a particular mode would 'cascade' through the mode space. Full MIMO equalization including all mode channels would therefore be required to compensate the modal coupling in a SI-MMF-MDM system.

As for the GI-MMF, its RI variation can be described as [26]:

$$n(r) = \begin{cases} n_1[1 - 2\Delta(r/R)^{\alpha}]^{1/2}, & r < R \\ n_1(1 - 2\Delta)^{1/2}, & r \geq R \end{cases} \quad (2)$$

where n_1 is the maximum RI of fibre core, Δ represents the relative RI difference between fibre core and cladding, and α is the profile parameter which determines the shape of RI profile. The value of α is set to 2 in the simulation, which indicates a parabolic RI profile as shown in Fig.1(b). The number of modes supported by the parabolic GI-MMF is $V^2/4$ [26]. The linearly polarized (LP) modes in the GI-MMF fall into MGs that share near-degenerate effective refractive index (n_{eff}), as shown in Fig.2(a), leaving a relatively large Δn_{eff} between different MGs. Such characteristics result in only weak inter-MG coupling, while the modes in the same MG are fully coupled because of their degeneracy. The intra-MG group delay spread in this strongly coupled regime can be calculated by means of the probability density function [8]. In this case, only the strong coupling among intra-MG modes needs to be considered in MIMO equalization, as the sufficiently large inter-MG Δn_{eff} can ensure negligibly small crosstalk between the MGs.

The RI profile for a SI-RCF with 20-µm core outer radius is shown in Fig. 1(c). The width W of the ring core can be limited to ensure only one radial mode is supported. Under this assumption, the number of (near-)degenerate modes included in each MG becomes fixed at 4 (except for the 0th-order MG which contains 2 modes). Fig.2(b) and (c) are representations of the RCF modes in the LP- and orbital angular momentum (OAM) modal basis [28], respectively. The LP-modes are formally given by:

$$LP_{l,1a}^{X} = HE_{l+1,1}^{e} + EH_{l-1,1}^{e} \quad (3a)$$

$$LP_{l,1a}^{Y} = HE_{l+1,1}^{o} - EH_{l-1,1}^{o} \quad (3b)$$

$$LP_{l,1b}^{X} = HE_{l+1,1}^{e} - EH_{l-1,1}^{e} \quad (3c)$$

$$LP_{l,1b}^{Y} = HE_{l+1,1}^{o} + EH_{l-1,1}^{o} \quad (3d)$$

whereas OAM-modes are

$$OAM_{l,R} = HE_{l+1,1}^{e} + jHE_{l+1,1}^{o} \quad (4a)$$

$$OAM_{-l,L} = HE_{l+1,1}^{e} - jHE_{l+1,1}^{o} \quad (4b)$$

$$OAM_{-l,R} = EH_{l-1,1}^{e} - jEH_{l-1,1}^{o} \quad (4c)$$

$$OAM_{l,L} = EH_{l-1,1}^{e} + jEH_{l-1,1}^{o} \quad (4d)$$

Although both are effective ways of describing RCF modes under the weakly guiding condition, there are subtle differences between them. The fact that LP-modes are composed of eigenmodes that are not strictly degenerate would have implications when the weakly guiding condition is not fulfilled, which is the case for some RCFs that will be reviewed later. The OAM-modes, however, are composed of eigen-modes that always maintain degeneracy. OAM-modes have either left- or right-handed circularly polarization (LHCP or RHCP) which manifest the spin angular momentum states of photons. They also have either left- or right-handed spiral phase front $\exp(\pm jl\phi)$ (where ϕ is the azimuthal angle of the fibre cross-section) which manifest the orbital angular momenta of photons with topological charge of $\pm l$ [29]. OAM modes therefore could be characterized as spin-orbital aligned (polarization and phase rotating in the same direction) as in Eq.4(a-b), and spin-orbital anti-aligned as in Eq.4(c-d). The use of different modal bases is largely a matter of launch and detection, as during propagation it is futile trying to distinguish between them. Yet, the LP- and OAM modes do have different propagation characteristics therefore using one or the other for launch/detection could result in different communications channel characteristics.

Similar to the GI-MMF, in RCFs strong coupling may occur among intra-MG modes while there is only weak coupling between different MGs separated by relatively large inter-MG Δn_{eff}. Therefore, MIMO processing would only be required to equalize the intra-MG modal crosstalk. It is noteworthy that the number of weakly-coupled MGs is determined by the core radius and the required inter-MG Δn_{eff}, which will be derived in section III. The inter-MG Δn_{eff} criterion used here for the RCF spectral efficiency (SE) and complexity calculation is $\Delta n_{eff} > 1 \times 10^{-4}$, which can ensure sufficiently small inter-MG coupling over 1-km fibre transmission so that the inter-MG crosstalk can be neglected in the simulation [9, 30].

B. Spectral-Efficiency and MIMO-Equalization complexity calculations and analysis

In MDM schemes, the MIMO channel matrices are equivalent to the mode transfer matrices in the fibre used [31]. The theoretical maximum SE supported by a fibre can therefore be calculated using the following equation based on the Shannon capacity theorem [32] and maximized by a water-filling algorithm [33]:

$$SE = \sum_{i=1}^{N} \log_2[1 + \frac{1}{P_{ni}}(\lambda_i \mu - P_{ni})^+] \qquad (5)$$

where i=1, …, N represents the mode channel number, P_{ni} refers to the noise power in each channel, λ_i is the singular value of the fibre mode transfer matrices for the i_{th} channel, μ is the water-filling power level and X^+ denotes max(X, 0).

The theoretical SE at SNR of 20 dB supported by the three types of fibres as shown in Fig.1 is plotted in Fig.3(a). According to this calculation, SI-MMF supports the highest SE (plotted as bands representing the range between weak to strong mode coupling conditions), up to 5-6 times higher over the other schemes at the standard MMF (e.g., OM4 fibre) core radius of R=25-µm, increasing further with the fibre radius. For GI-MMF and RCF MDM schemes, the predicted SE values are surprisingly very similar. This is because, despite the fact that RCFs support fewer modes by limiting radial mode number to one, their *effective* degree of freedom (EDoF) [34] – namely number of channel with good SNR – are similar to that in GI-MMF.
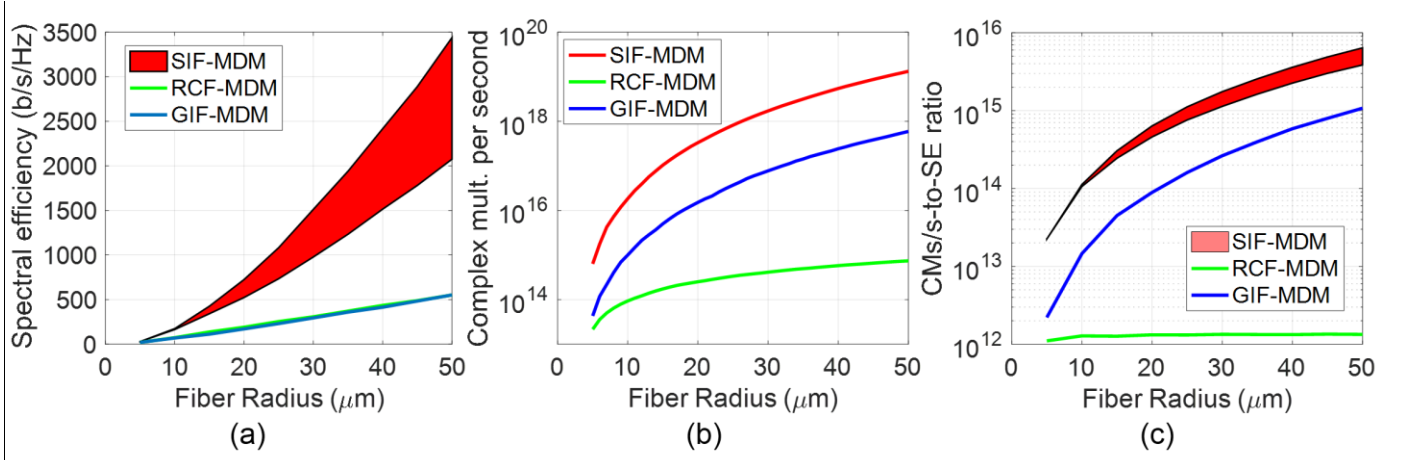

Fig. 3 (a) Spectral efficiency ;(b) total complex multiplications per second; (c) complexity-to-SE ratio at different fibre-core radius for different MDM schemes implemented on various fibres at SNR of 20 dB after 1-km transmission.

As for the MIMO-equalization complexity calculation, we assume the use of single-carrier adaptive frequency-domain equalization (FDE) to mitigate the linear impairments resulted from mode coupling [2]. The complexity of $N \times N$ finite impulse response (FIR) filter-based FDE can then be measured by the number of complex multiplications (CMs) per second as [6]

$$CM = \frac{(2+N)N_{FFT} \cdot \log_2(N_{FFT}) + 2N \cdot N_{FFT}}{(N_{FFT} - N_{MD} + 1)} R_s \qquad (6)$$

where N_{FFT} is the fast Fourier transform (FFT) block length, R_s is the symbol rate, and the oversampling ratio per symbol equals to 2. In order to realize the adaptive filter update, we assume a 50% overlap-save FFT being used to avoid cyclic prefix. N_{MD} is the number of filter taps for each equalization block due to the DMD between modes. Here we assume chromatic CD can be totally compensated before the FDE, leaving modal coupling and DMD as the major contributing factors to the complexity.

The CMs per second needed to support the above theoretical SE over a 1-km fibre are shown in Fig.3(b). Here we assume the MDM schemes are populated by 32 GBaud QPSK signal channels until the SE as plotted in Fig.3(a) is fully exhausted. According to the results in Fig.3(b), SI-MMF requires two orders of magnitude higher CMs per second over RCF-MDM while its SE is only a factor of ~ 6 higher [as shown in Fig.3(a)].

The significantly reduced complexity in RCF-MDM results from the use of intra-MG MIMO that is at a fixed 4x4 scale for all high-order MGs. In contrast, in the GI-MMF MDM scheme, intra-MG MIMO complexity will still increase albeit at a much lower rate than SI-MMF, resulting in a MIMO complexity that is one order of magnitude higher over RCF.

One can also use the complexity-to-SE ratio to evaluate the number of CMs per second required to achieve 1 b/s/Hz of SE. As the results in Fig.3(c) indicate, at the SNR of 20dB and in the core radius range of 5-50 µm, the RCF-MDM system is by far the most computationally efficient of all the three schemes, at least 10× more efficient than GI-MMF MDM and 100× more efficient than SI-MMF MDM systems. These results predict that RCF-based MDM scheme should have the best scalability as it provides SE comparable to GI-MMF systems while requiring the lowest MIMO-equalization complexity, and thus the lowest DSP cost and power consumption, provided that the low inter-MG coupling can be maintained when the number of MGs is increased. It also has the advantage that the MIMO scale is fixed, therefore can be modularly upgraded with no need to implement more complex MIMO when expanded towards higher order MGs.

The need for the 4x4 MIMO within each MG could be further eliminated if the degeneracy between the 4 eigen-modes belonging to the same group could be broken, so that a relatively substantial $\Delta\beta$ or Δn_{eff} exists between them to

warrantee sufficiently low intra-MG coupling within the transmission distance. This would result in extremely low signal processing complexity as modes become independent channels. Such a strategy has been targeted by some specially designed RCFs for further lower MIMO-equalization complexity or even MIMO-free transmission, which will be discussed in the following sections.

C. Challenges for Practical RCF-based MDM Systems

There are several major challenges in the practical implementations of RCF-based MDM systems that attempt to tap into the predicted low complexity afforded by its mode-group partition and fixed-size modular MIMO. Among these, high quality RCFs, efficient mode (de)multiplexers (DEMUX), and RCF-based MDM amplifiers are likely to be the most important components, while system architecture also plays an important role especially set against potential applications scenarios. We will review the progress made in RCF design and fabrication, DEMUX devices, as well as RCF-based MDM transmission experiments in the following sections.

III. DESIGN AND FABRICATION OF RCFs

In this section, focusing on the circular cylindrical RCFs, we firstly discuss in detail how the design parameters affect the fibre characteristics with emphasis on RCF design schemes aiming at decreasing modal coupling and fibre attenuation. Polarization-maintaining RCFs, specially designed to further break the degeneracy between adjacent modes are also reviewed at the end of this section.

A. Circular Cylindrical RCFs

1) Main Design Parameters

The RI distribution of a cylindrical RCF design is governed by three main parameters: the average ring core radius (R), the ring core width (W) and the core-cladding index contrast ($\Delta n = n_1 - n_2$). It can be derived that the effective refractive index difference Δn_{eff} between adjacent MGs is related to their topological charge $l_{1,2}$ (i.e., the azimuthal mode index) and average ring core radius R by:

$$\Delta n_{eff} \approx \left[\frac{\lambda_0}{2\pi R}\right]^2 \frac{l_1 + l_2}{n_{eff1} + n_{eff2}} \qquad (7)$$

This equation indicates that the Δn_{eff} between a pair of adjacent MGs should increase approximately linearly with their topological charge values (i.e., MG order), leading to larger Δn_{eff} between higher order MGs. When Δn is fixed (e.g., limited by achievable material parameters in manufacturing), R will largely determine the inter-MGs Δn_{eff} because an RCF with larger R supports more MGs with smaller inter-MG Δn_{eff}, while the total number of MGs supported by an RCF is limited by the condition of $n_{eff} > n_2$. The ring width W are usually chosen so that for all azimuthal mode index l values, the radial mode index remains one. Within this restriction, a thicker ring (larger W) would support more MGs and provide less attenuation by shifting all n_{eff} values of all MGs up towards n_1.

In addition to R, W, and Δn, the RI distribution has profound effects on the characteristics of RCFs, and very much distinguishes two different approaches to RCF design and the

optical transmission system architecture implemented over these.

2) RCFs supporting MIMO-free OAM transmission

Excellent reviews of RCF fibres designed for OAM transmission can be found in [30, 35]. Here we only briefly summarize some key points.

Following a first-order perturbative analysis, the eigen-values of modes in the same MG should be modified by a correction factor written as [36]

$$\Delta\beta^2 \approx \frac{-\int_{tot}\left(\bar{\nabla}\cdot\bar{e}\right)\left(\bar{e}\cdot\bar{\nabla}\left(\ln n^2\right)\right)dA}{\int_{tot}\left|\bar{e}\right|^2 dA} \qquad (8)$$

where vector $\vec{e}$ is the modal electrical field. Eq.(8) indicates that a profound role is played by the radial gradient of the RI distribution - by collocating large RI gradient with high field, a split in eigen-values ($\Delta\beta$ or Δn_{eff}) between the near-degenerate EH and HE modes can be achieved, therefore separating the spin-orbital aligned and spin-orbital anti-aligned OAM modes sufficiently so that they could propagate with low coupling as indicated by Eq.(1). As each now contains two OAM modes with orthogonal polarization states, transmission of a polarization multiplexed (PolMux) coherent optical signal (as currently implemented over SMF) can be implemented over each. In this sense, the scheme is free of additional MIMO on top of what's already contained in the PolMux receiver for equalization of polarization coupling. Clearly, these RCFs, optimized for OAM transmission, are not suitable for LP-mode based MDM schemes. If data channels are launched and detected as LP modes, the increased walk-off between HE and EH mode will result in extremely profound frequency-selective fading in the channel response. It is therefore appropriate for these fibres to be known as OAM fibres.

Such OAM fibres can be engineered by having specially designed RI profile and also by maximizing Δn between the ring core and the inner or outer cladding. Solid silica fibre technology can achieve a maximum Δn of ~0.03 or relative RI contrast of ~ 2% (with both Germania and Fluorine doping). The highest number of OAM modes reported in solid silica fibre is 8. With Δn_{eff} values typically of 1.4×10^{-4}[37], solid silica OAM fibres are likely only be able to sustain transmission distances in the km scale before crosstalk becomes too high. Indeed, all reported single span data transmission distance of such OAM fibres are in the 1-2 km range.

Some structures, in particular air inner cladding (often known as air-core), micro-structured, and polymer fibres, can provide high Δn and high RI gradient. Air-core OAM fibres in particular have been reported to support up to 6 modes over transmission distance of 13.4km, or 12 modes over 1.2km, with Δn_{eff} values up to 1.7×10^{-4} [38,42]

Although high Δn enables high mode number and large intra-MG mode split, it could also cause high attenuation due to increased susceptible to scattering, therefore requires very high fabrication quality. Recently an air-core RCF has been reported with relatively low loss levels of ~0.8 dB/km [38].

Another interesting effect found in very high RI gradient air-

core RCF is spin-orbital coupling which gives rise to so-call non-integer OAM modes with elliptical polarization states [39]. This in theory is not a problem for MDM transmission as long as modes maintain their orthogonality and are launched with the correct non-integer spin-orbital state.

3) RCFs supporting modular MDM and MGM transmission

A contrasting approach to the OAM fibre, derivable from Eq.(8), is that low RI gradient designs can be used to increasing the intra-MG degeneracy [40] by significantly reducing the $\Delta\beta$ or Δn_{eff} between the HE and EH eigen-modes, which in turn results in strong intra-MG coupling that would further reduce DMD [41] and compress impulse response. Consequently, using either the OAM mode basis or the LP basis for launch and detection presents little difference in terms of the MDM channel characteristics [42]. This type of RCF supports transmission schemes either based on the low complexity 4x4 modular MIMO scheme as proposed in section I, or mode group multiplexing (MGM) schemes using the entire MG as a single channel. The latter is possible because the intra-MG degeneracy ensures that the MG as a communications channel has a flat wideband frequency response. In the following, we will mainly discuss the design and optimization of this type of RCF.

Several RCFs with various *R, W, Δn* and RI profile have been reported. In 2015, Fujikura reported [43] a RCF of 11.2 km length that supports LP_{01} (*l*=0) and LP_{11} (*l*=1) modes with Δn_{eff} of 1.0 and 1.4×10^{-3} at 1350 and 1550nm, respectively. Its LP_{01} and LP_{11} modes have attenuation of 0.235 and 0.239 dB/km respectively. They also found that coupling coefficient converges to a constant value of 7.4×10^{-5} km^{-1} when Δn_{eff} exceeded 1.7×10^{-3}. This level of coupling coefficient should support low crosstalk of < -20 dB over 100 km.

RCFs supporting 5 and 7 MGs was reported by Jin et al of the University of Southampton, UK [22]. These had *R* values of ~ 6 and 11 μm, respectively, with Δn of ~ 0.015. Both had a graded RI profile of

$$n_0(r) = \begin{cases} n_a\left[1-2\Delta\left(\frac{r-r_a}{W/2}\right)^{\alpha}\right]^{1/2} & |r-r_a| \le W/2 \\ n_a\left[1-2\Delta\right]^{1/2} & |r-r_a| > W/2 \end{cases} \quad (9)$$

with *W* of ~ 8 and 5 μm, respectively. The 5-MG fibre demonstrated attenuation of ~ 0.7-1 dB/km for MG 1-4 and coupling coefficient that decreased (as expected) between higher order MG, reaching $< 2\times10^{-1}$ km^{-1} between MG3-4 and MG4-5 respectively. The 7-MG fibre on the other hand had very high loss of >100 dB/km and very high coupling coefficients of 10 - 100 km^{-1} between MGs (and *increased* between higher order MGs). This high attenuation and high loss has been attributed to the increased susceptibility to micro-bending when *R* is increased, despite that both fibres had the same σ of ~ 35 nm.

In 2017, Yung et al [44] of the same group reported a 25.2 km long RCF with Δn of ~ 0.0135, *R* of 5.55 μm and *W* of 3.5 μm. Although designed as a 'step-index' RCF, the measured RI profile is actually profoundly graded, closer to α=3.3. This fibre supported four MGs of LP_{01-31} (MGs *l*=0 to 3), with attenuation

of 0.29-0.32 dB/km, and Δn_{eff} of $> 2\times10^{-3}$ for MGs of LP_{11-31}. The authors of this paper reported a GI-RCF [39, 45] with parabolic profile of α=2 in Eq.(9), with Δn of ~ 0.025 (achieved by both Ge- and F-doping), *R*=7.6 μm, and *W*=3.8 μm. This fibre supported six MGs (*l* = 0 to 5), with inter-MG $\Delta n_{eff} > 2\times10^{-3}$ between MGs of *l* = 3, 4, and 5. Coupling coefficients of 4.7 and 9.3 $\times10^{-3}$ km^{-1} was measured between MG4-5 and MG3-4, respectively. The overall attenuation was first reported [39] as 1 dB/km for all guided modes in a 10-km specimen, but has since been re-measured as 0.75 dB/km over an 18-km specimen [28]. A remarkable feature of this design is that the intra-MG Δn_{eff} has been minimized to $\sim1\times10^{-5}$ due to the low RI gradient design. This results in very low DMD for minimized MIMO complexity in MDM transmission and flat broadband response as MGM channels. The relatively high inter-MG coupling coefficient compared with the Fujikura result, and the higher attenuation compared to Fujikura and Southampton results can be attributed to the fact that the fabrication process was slightly flawed that caused unintended fluctuations in the RI distribution. These fluctuations also likely have caused the higher than expected coupling coefficient. In the following section, a discussion of potential approaches of optimizing RCFs for low coupling and low loss will be given.

4) Optimization of RCFs for MDM and MGM transmission

The main optimization targets of RCFs for MDM / MGM transmission include: (1) minimizing the inter-MG coupling so that low inter-MG crosstalk is maintained over long distances, (2) maximizing the number of low-crosstalk MGs so that the total capacity can be maximized, and (3) minimizing the RCF attenuation for longer transmission distance. Low intra-MG DMD is also desirable as already addressed above.

Under the restriction of achievable Δn in solid silica fibres, to increase the number of MGs (by means of increasing *R*) inevitably reduces the inter-MG Δn_{eff}. According to Eq.(1), low inter-MG Δn_{eff} could lead to higher inter-MG Coupling coefficient or crosstalk, and possibly high attenuation, unless the other factors can be addressed effectively.

Two important approaches for decreasing the inter-MG coupling are implied by Eq.(1) in addition to maximizing inter-MG Δn_{eff}. Firstly, fibre RI profile should be optimized to reduce the overlap integration between the modal fields and the RI gradient. Secondly, fibre quality should be improved to reduce σ and κ that are strong contributing factors to both the crosstalk and fibre loss. While σ is a summary description of the magnitude of the RI perturbations in the fibre and could be minimized by improved fibre fabrication techniques, how to counter the effects of inevitable perturbations can be inferred by an extension of conventional fibre perturbation theory.

The coupling coefficient between two propagating modes is expressed as the integral over the product of their electrical fields and the RI perturbation, $E_1[n(x,y,z)-n_0]E_2$, in the fibre cross-section (r,ϕ) plane [46]. For simplicity, the micro-perturbations (e.g. micro-bending) can be assumed to only affect the RI distribution in the *x*-direction (*x-y* being the transverse plane while *z* the propagating direction). While conventional micro-bending analysis works by implementing a 1st-order Taylor expansion of the RI perturbation [27], much can be revealed by extending the Taylor series to the 2nd-order:

$$\Delta n(x,y,z) = n\big[x_0 + f(z), y_0\big] - n_0(r)$$

$$= \frac{\partial n_0}{\partial r}\cos\varphi\, f(z) + \frac{1}{2}\left[\frac{\partial^2 n_0}{\partial r^2}\cos^2\varphi + \frac{1}{r}\frac{\partial n_0}{\partial r}\sin^2\varphi\right]f(z)^2 \tag{10}$$

where n_0 is the original RI distribution and $f(z)$ is the random perturbations in the x-z plane.

Substituting Eq.(10) into Eq.(1) and focusing on the angular integral part, one finds that the 1st-order Taylor term as a linear function of $\cos(\varphi)$ only contributes to the coupling between adjacent MGs (n-$m = l_1$-$l_2 = 1$) because only the product of E_1 and E_2 of adjacent MGs have the term $\exp(\pm i\varphi)$ that makes the angular integral non-zero. Similarly, the 2nd-order Taylor term only contributes to the coupling between the next nearest neighbouring MGs (i.e., l_1-$l_2 = 2$). These two terms are the main sources of the optical crosstalk in RCFs, as MG farther away are partitioned by very large Δn_{eff}. It should be noted that the fibre attenuation can also be analyzed using the same process, where the coefficient represents the coupling between guided core modes and radiative cladding modes [46].

The implication of above analysis is that the RI distribution of the RCF can be optimised to minimise coupling caused by micro-perturbations if it can be designed such that the their overlap integral of the 1st- and 2nd-order Taylor terms and the field are minimal. Attenuation should also be minimized in the same process as less energy 'cascades' through the MGs to reach the cladding modes that is coupled to the two highest order MG through the same mechanism. For example, a minimized overlap integral between the field and the 1st-order Taylor term can be achieved through having a RI gradient of zero (which is non-physical) or having a positive and negative RI gradient that cancel out each other, as the field is always positive due to the radially single mode condition. Unlike SI- or GI-MMF, RCFs naturally have a rising and falling edge in its radial RI distribution, hence are conducive to such designs. Similarly, by careful engineering RI distribution it should also possible to further minimize the overlap integral between the field and the 2nd-order Taylor term for low coupling between next-nearest neighbouring MGs.

5) Guided and available MG number for MDM

The number of guided MGs (l_{max}) in RCFs can be estimated by assuming a SI-RCF structure and applying the principle pf momentum conservation to the guide modes, meanwhile removing the factor $(2\pi/\lambda_0)^2$ on both sides of Eq.(7) as $k=(2\pi/\lambda_0)n$:

$$n_{eff\,l}^2 + \left(\frac{\lambda_0 l}{2\pi R}\right)^2 + \left(\frac{n_1^2 - n_2^2}{4}\right) \le n_1^2 \tag{11}$$

where the term with coefficient 1/4, corresponding to the radial momentum, is derived from the radial single index restriction with Eq. (7). Using the condition of $n_1 > n_{eff} > n_2$ in Eq.(11), the maximum value of l, or guided mode number, can be calculated, and is mainly related to R and Δn when W is fixed.

It is important to note that, although the guided mode number increase monotonously with R, the mode number *available* to MDM application is restricted by the inter-MG Δn_{eff} value needed to keep inter-MG crosstalk low. It is therefore directly linked to what Δn_{eff} values are needed for low crosstalk transmission over certain distances. As indicated in literature [9, 30], Δn_{eff} values of 1×10^{-4}, 1×10^{-3} and 2×10^{-3} may be needed for 1-, 10- and 100-km distance transmission while keeping inter-MG crosstalk below -20 dB.

Note that Δn_{eff} between adjacent MGs increases linearly with MG index l, RCFs may be designed so that only higher order modes satisfied above required inter-MG Δn_{eff} criteria, which means that MGs available for MDM transmission could be fewer that the total number of guided MGs. As core radius R is increased, this available MG number (each MG containing four near-degenerated modes) at $\Delta n = 0.02$ is plotted in Fig.4 for inter-MG Δn_{eff} values of 1×10^{-4}, 1×10^{-3} and 2×10^{-3}. A notable feature of this analysis is that the available MG number has a maximum. For the case of $\Delta n_{eff} = 2\times10^{-3}$, a maximum of 11 MGs is reached at $R = 18\sim26$ μm, providing 44 MDM channels in a single ring core. For Δn_{eff} of 1×10^{-3}, the maximum available MG number of 22 (or 88 MDM channels) is reached at $R=35$ μm. Further increase of R beyond the maxima will only reduce the number of available MG as the inter-MG Δn_{eff} further reduces. If only 1×10^{-4} is required, even more MGs could be available at larger R, usable either as MIMO-free MGM channels or modular MIMO MDM channels.

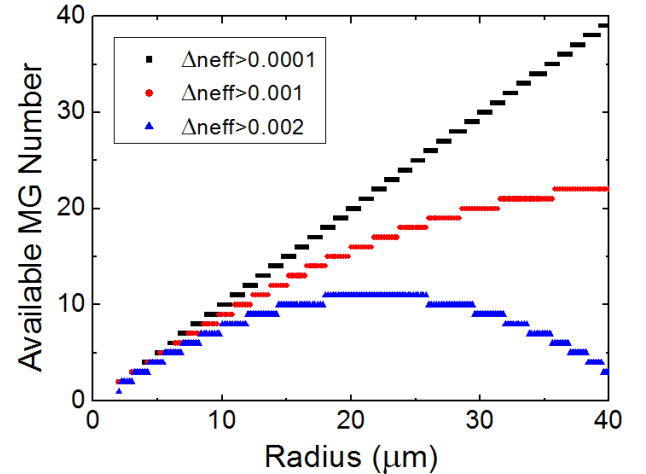Fig. 4 Number of available MGs in a single RCF at $\Delta n = 0.02$ satisfying $\Delta n_{eff} > 1\times10^{-4}$, 1×10^{-3} and 2×10^{-3}, respectively, as a function of core radius.

These theoretical results - that the RCF could indeed support substantial capacity increase of 1-2 orders of magnitude over SMF for long- or short-reach transmission - should be viewed with caution, as it is not yet clear how modes would behave at large R. Some initial study [22] points to possible instability at large R, but further investigation is needed.

B. Polarization-Maintaining RCFs

In order to further break the degeneracy between the odd and even vector modes with the same order in the circular cylindrical RCF and thus simplify or eliminate the MIMO processing, polarization-maintaining (PM) designs have been introduced to the RCF recently, including the elliptical RCFs and the PANDA RCFs.
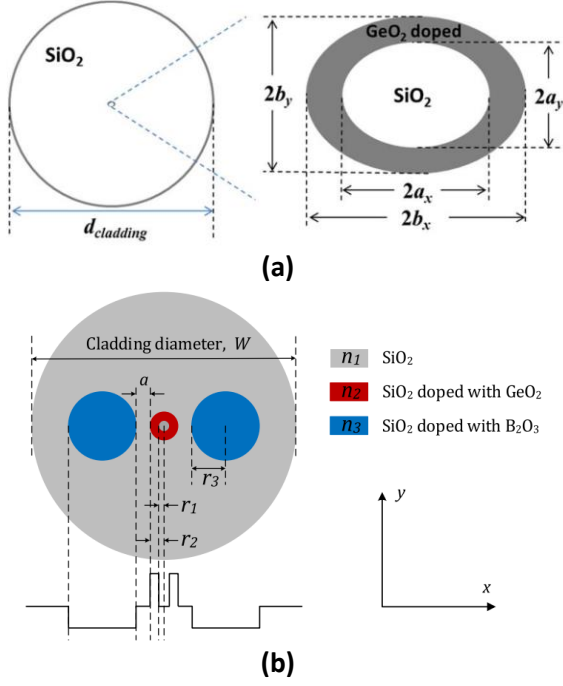
Fig. 5. Schematic diagram of the cross section for (a) the elliptical RCF[47] and (b) the PANDA RCF[49].

Compared with the elliptical FMF, the target of intra-MG $\Delta n_{eff} > 10^{-4}$ can be achieved at a smaller ellipticity in RCFs, which mitigates the cut-off of the high-order modes and thus the trade-off between effective index separation and the number of modes existed in the elliptical FMF [47]. Several elliptical RCF designs with relatively more guided vector modes and large enough Δn_{eff} to break the modal degeneracy have been proposed recently. L. Wang *et al.* [47] proposed an elliptical RCF design that could support up to 10 guided vector modes over the entire C band and eight higher-order vector modes were all separated from their adjacent modes by $\Delta n_{eff} > 10^{-4}$, except for the two fundamental modes, as its schematic diagram of the fibre cross section shown in Fig.5(a). In order to further separate the two fundamental modes, J. Zhao *et al.* proposed a design of elliptical RCF utilizing a central circular air hole which could support 14 distinctive polarization modes including the two fundamental modes with adjacent modal $\Delta n_{eff} > 1.2 \times 10^{-4}$ (including the fundamental modes) over the whole C+L band [48].

Aiming at avoiding the cut-off of the higher-order modes in elliptical-core fibres with high ellipticity, H. Yan et al. presented a polarization-maintaining PANDA RCF design by the combination of a ring-core structure with two stress-applying rods. Using a high-contrast index ring and stress-induced birefringence, the PANDA RCF could support 10 vector modes with Δn_{eff} among adjacent modes $> 10^{-4}$ over a wide wavelength range from 1500 to 1630 nm [49]. The geometry of the cross section for the designed PANDA RCF is shown in Fig. 5(b). Y. Cao et al. then improve this PANDA RCF design to support 16 weakly coupled LP-modes with $\Delta n_{eff} > 10^{-4}$ among adjacent modes [50] .

IV. Optical Mode Multi/Demultiplexers for RCFs

Spatial mode (de-)multiplexers (MUX/DEMUX) are critical components of MDM systems. Mode MUX combines input signals from N independent SMFs into N orthogonal modes of the transmission fibre, while the mode DEMUX separate these signal-carrying orthogonal modes into N output SMFs. In general, an ideal spatial mode MUX/DEMUX should be lossless, low-crosstalk, and scalable. In other words, it should perform a unitary transformation between the MDM fibre mode-set and the collective mode-set of multiple spatially shifted SMF, irrespective of the number of mode channels involved. The MUX/DEMUX should also be broadband (to be WDM compatible) and compact.

Many kinds of mode-selective MUX/DEMUX devices have been proposed and demonstrated for the RCF-based MDM systems, which can be divided into three categories.

A. Free-space optics MUX/DEMUX

In the early stage of MDM research, spatial mode MUX/DEMUX were often based on free-space optical elements of multiple phase plates and beam splitters to convert each targeted spatial mode separately and then combine them together [30]. This scheme is straightforward to implement, but the large number of optical elements and high insertion loss make it impractical in practical applications. Approaches based on free-space optical elements for OAM mode multi/demultiplexing include interference with Dove prisms [51] and spin-to-orbit conversion with q-plates [52]. However, the scalability of these schemes and their compatibility with fibre communication systems need to be improved.

A simpler OAM (de-)multiplexing scheme was proposed based on the Dammann vortex grating [F2], which imparted desired topological charges to diffracted beams at different diffraction orders and therefore could be used to demultiplex input OAM modes to Gaussian modes at the corresponding diffraction orders. As only one phase mask is required, this scheme is much more compact compared with other free-space phase-plate based MUXs/DEMUXs. However, a drawback of this scheme is the inherently high insertion loss of $10\log_{10}(1/N)$ for (de)multiplexing N modes, namely, it is not a unitary transformation.

Mathematically, an orthogonal mode set can always be losslessly converted to any other orthogonal mode set with a unitary transformation. This was found to be achievable with a succession of spatial phase modulations and Fourier transformations [53], as shown in Fig.6(a). Based on this idea, a multi-plane light conversion (MPLC) scheme was proposed for mode multi/demultiplexing, which could (de)multiplex any mode set with no intrinsic loss in principle [54, 55]. A 10-mode MPLC based MUX/DEMUX between SMFs and a MMF was implemented with average mode crosstalk of -21dB and insertion loss of -4.4dB [55], achieving high mode selectivity and efficiency. However, $2N+1$ phase plates were required for N-mode multi/demultiplexing in this scheme after optimization [54], resulting in increasing device complexity as the number of modes increases.
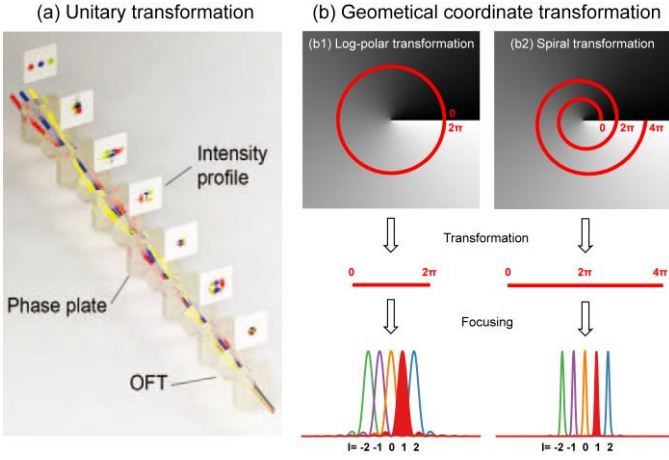
Fig. 6. Spatial mode multi/demultiplexing by free-space mode conversion base on (a) a general unitary transformation [55] and (b) geometrical coordinate transformations particularly for OAM mode sorting including the (b1) log-polar transformation and (b2) spiral transformation [57].

Nevertheless, in the case of (de-)multiplexing OAM modes which has simpler symmetry, there exist more elegant and easy-to-implement spatial transformations known as geometrical coordinate transformations as illustrated in Fig. 6(b) [56, 57]. A log-polar coordinate transformation, in which log-polar coordinates in the input plane are conformally mapped to Cartesian coordinates in the output plane, was introduced for OAM mode sorting [56]. It can be performed with only two phase-masks and a Fourier transformation lens. After propagating through this system, the spiral wave-front of an input OAM mode is transformed to a tilted plane wave-front with the tilt angle proportional to the OAM mode topological charge. OAM modes with different topological charges are hence transformed to plane wave-fronts with different tilt angles which can be focused to distinct positions in the focal plane of the lens. This scheme is a true unitary transformation that maintains its simplicity regardless of mode numbers. However, the log-polar transformation suffers high mode crosstalk due to significant overlap between adjacent demultiplexed modes, as shown in the lower-left part of Fig.6(b). To overcome this problem in principle, the authors proposed and demonstrated a novel 'spiral transformation' very recently, which is able to perform the same OAM (de-)multiplexing function with significantly higher resolution and thus lower mode crosstalk, as shown in Fig. 6(b2)[57], also with only two phase masks.

Despite their simplicity, geometrical transformation DEMUX devices still need to address problems of mode mismatch with SMF, as they transform OAM modes into elongated stripes rather than circular Gaussian modes. This could be corrected by incorporating further phase correction into the second phase mask, or into the Fourier transformation lens by implementing it also as a phase mask.

B. Waveguide-based Integrated MUX/DEMUX

Mode MUX/DEMUX for RCF-based MDM systems have also been demonstrated based on photonic integrated circuit (PIC) platforms due to their potential capability of miniaturization and mass production.

Much research has been focused on MUX and DEMUX for the OAM mode-set. The first demonstrated silicon PIC OAM MUX/DEMUX, as shown in Fig. 7(a), consists of a circular grating coupler and a multi-port star coupler, which are connected through phase-matched waveguides [58]. A similar device is also demonstrated in a free-space OAM communication system [59]. The core idea inside these devices is similar to the geometrical coordinate transformation discussed before [56, 57], which converts the vortex phase into a linear titled phase that can be subsequently focused to a specific lateral position. The geometrical transformation that convert the sampled vortex phase into a linear phase is realized by arranging the phase-matched array waveguides from a circular formation to a linear formation, while the star coupler functions as a Fourier transformation lens that focuses the tilted wave-fronts into different lateral output ports. However, this silicon PIC suffers from relatively high mode crosstalk of ~ -7 dB [59] and also large coupling loss of about 11.2 dB to RCF [58]. To alleviate this problem, a similar device fabricated in a silica planar lightwave circuit (PLC) platform combined with 3D waveguide circuits to avoid vertical grating coupling was demonstrated later as shown in Fig.7(b) [60].

Another family of OAM MUX/DEMUX based on micro-ring resonators with embedded azimuthal angular gratings [61] have been researched. Its underlying principle is that the whispering gallery modes (WGM) supported by a micro-ring resonator can be extracted and converted into radiated OAM modes through the angular grating, with the output topological charge strictly defined according to the azimuthal phase-matching condition leading to high mode purity. Since each micro-ring can only emit one OAM mode, in order to multiplex more OAM modes, two schemes have been proposed and demonstrated [62, 63]. One is to vertically integrate multiple concentric micro-ring resonators using wafer bonding technique as shown in Fig. 7(c) [62] and the other is realized by breaking a complete micro-ring to configure an Ω-shaped waveguide so that multiple concentric devices can be integrated without crossing between the access waveguides, as shown in Fig. 7(d) [63]. However, a common drawback of ring-waveguide devices is that they rely on phase-matching condition, and thus are wavelength dependent. Therefore, their compatibility with broadband WDM is restricted.

A common feature of above circularly distributed waveguide OAM emitter is that they emit vector modes that are either predominantly tangential or radial polarized, which is not matched to RCF's circularly polarized OAM modes. Recently the authors addressed this problem by engineering the so-called 'transverse spin' in the evanescent wave region of silicon nitride micro-ring waveguides, achieving arbitrary control over the emitted OAM mode SoP [64]. A silicon PIC-based circular-polarized OAM MUX/DEMUX targeting direct chip-to-fibre coupling was also proposed recently [65].

Planar integrated LP mode MUX/DEMUX devices have also been widely researched, although not necessarily for RCFs only. A typical device was reported in [66], where a number of waveguide grating couplers are arranged in formations that matches the LP mode distribution. The same principle can be used for RCF LP mode DEMUX, although for higher order modes the number of gratings will increase as at least $2l+1$ gratings will be needed to excite the l-th MG. While launching

LP- or OAM modes are similar in their complexity, for RCFs demultiplexing OAM modes is generally easier to implement than demultiplexing LP modes, because azimuthal alignment would be necessary between LP modes and the DEMUX device.
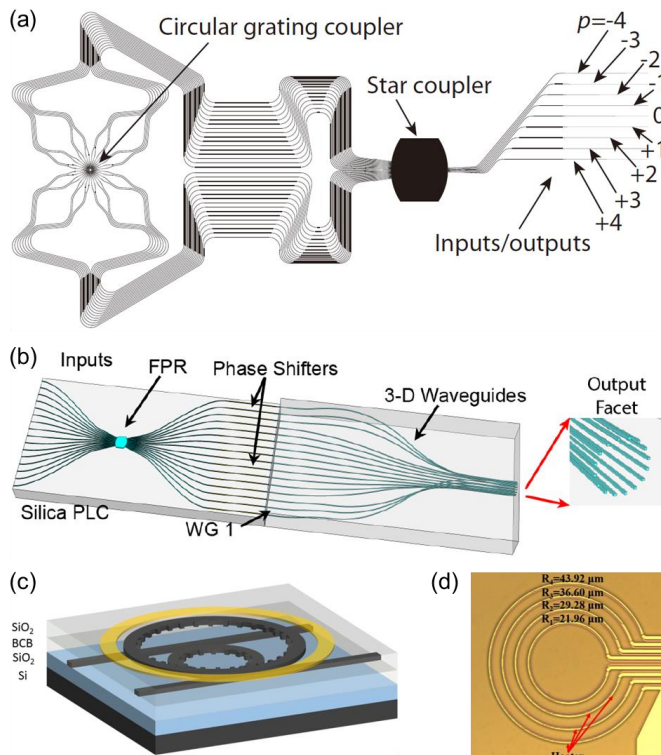

Fig. 7. Different kinds of photonic integrated devices for OAM multi/demultiplexing. (a) Silicon PIC [58]; (b) Hybrid device consisting of a silica PLC and a 3D waveguide circuit [60]; (c) Vertically integrated device of concentric micro-ring resonators with embedded angular grating [62]; (d) Concentric Ω-shaped waveguide device with embedded second-order Bragg gratings [63].

C. Fibre based MUX/DEMUX

All-fibre mode-selective MUX/DEMUX devices are desirable in MDM systems as their direct splice to transmission fibres without fibre-free-space-fibre or fibre-chip-fibre coupling, which could enable mode (de-)multiplexing with high stability and low insertion loss. A number of fibre-based MUX/DEMUX devices for RCFs have been proposed or demonstrated recently [67-72].

The first kind of all-fibre MUX/DEMUX devices are based on optical fibre couplers, which include two types as shown in Fig.8(a, b). The first type is implemented by using a spot-based coupler shown in Fig. 8(a) [67], which employs multiple SMF ports equally distributed on a circle to sample the transverse profiles of modes in the RCF. In this way, different RCF modes or their combination can be excited by controlling both the amplitude and phase of light from the SMF input ports. Although the underlying principle in this design is straightforward, high mode-dependent loss and crosstalk may result from the fact that higher order RCF modes inherently require more sampling points. The other type is a mode-selective coupler shown in Fig.8(b) [68], in which selectively

coupling between different modes in the RCF and the SMF mode is realized through phase matching between the modes. Based on this scheme, S. Pidishety et al. demonstrated an all-fibre mode-selective coupler capable of exciting two OAM modes ($l = \pm1$) with about 6-dB insertion loss and 72% mode purity over 1-nm spectral range at ~1550 nm. In order to multiplexing more OAM modes, a cascaded-coupler configuration may be used.

The other category of all-fibre MUX/DEMUX devices is based on photonic lanterns (PLs), which are a kind of passive fibre/waveguide components that adiabatically merges multiple single-mode fibres or waveguides (SMFs/SMWs) into one multimode fibre/waveguide (MMF/MMW), aiming at efficient mode conversion between them [69]. For mode (group)-selective PLs, dissimilar input SMFs/SMWs may be employed, so that each input fibre excites only one mode (group) in the MMF/MMW [2]. In order to realize a ring core PL compatible with RCFs based on the existed PL fabricating technique, Z. S. Eznaveh et al. demonstrated a strategy by replacing the central input SMF with a core-less fibre so as to create low refractive index in the centre, as shown in Fig. 8(a) [70, 71]. In this work, five input SMFs were designed to excite the first five LP modes and OAM modes up to the second order could be generated through simultaneous excitation of two degenerate LP modes to constitute an OAM mode. By splicing the end-facet of this ring core PL to a RCF, coupling loss of <3dB could be achieved for all the five OAM modes, but the mode crosstalk, a critical issue of this kind of devices, still requires further investigation.

In addition to the above approaches, still more schemes, such as an MMI-based MUX/DEMUX consisting of a RCF and a fixed phase array, have been proposed as shown in Fig.3(d) [72]. The implementations of these schemes are still under way.
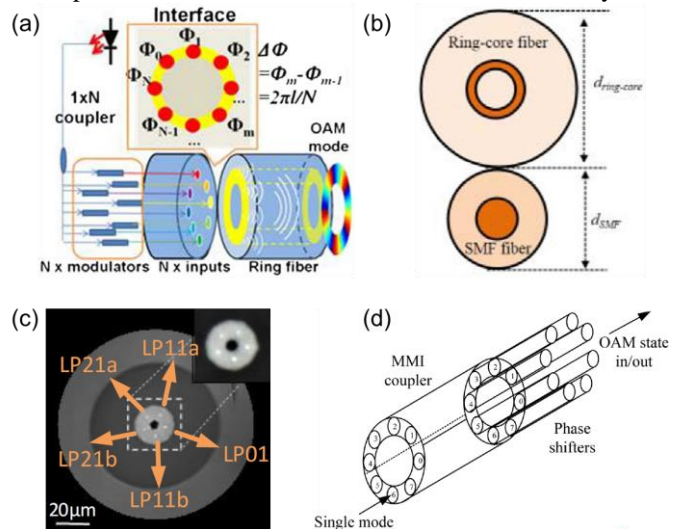
Fig. 8. All-fibre OAM MUX/DEMUX toward RCFs based on (a) spot-based couplers [67], (b) mode selective couplers [68], (c) mode selective photonic lanterns [71] and (d) MMI-based fibre devices [72].

V. RCF BASED OPTICAL AMPLIFIERS

Compared with MMF/FMF based amplifiers, it is easier to achieve low differential mode gain (DMG) in RCF amplifiers due to the high similarity between the profiles of different RCF modes, resulting in similar overlap integrals between different

modes and the optical gain profiles. Currently reported RCF-amplifier schemes can be divided into two kinds.

A. RCF-Based Erbium doped fibre amplifiers (EDFAs)

Similar to SMF communication systems, EDFAs can provide efficient solutions to extend the transmission distance of the RCF-MDM systems. H. Ono *et al.* first demonstrated a two-LP-mode RCF EDFA [73]. As shown in Fig.9, its ring-core RI profile, in which Erbium ions were doped in the high-refractive index area, enable very similar overlap integrals with both the LP_{01} and LP_{11} mode profiles. As a result, there was at least 4.5-dB improvement for the DMG of the RCF-based EDFAs, compared with that of the SI-FMF-based EDFA. They also extended the concept to the multicore-RCF-based EDFA, showing good performance at differential modal/core gain [74]. Y. Jung *et al.* demonstrated an OAM amplifier with topological charge $|l|$=1 for the first time by utilizing an air-core EDF with a cladding-pumped configuration, in which up to 15.7-dB gain was achieved within the wavelength range of 1545-1600nm [75]. They later also reported a EDFA base on a GI-RCF [76], achieving < 1-dB DMG for five LP modes belonging to three MGs, which is the lowest DMG experimentally measured from any few-mode EDFA so far.
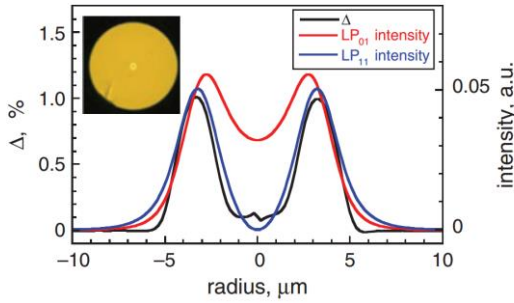

Fig. 9. RI profile and intensity profiles of LP_{01} and LP_{11} mode signals of the two-mode RCF-based EDFA [73].

The pumping configuration (core or cladding pumping), erbium doping distribution, and the RI profiles all have an impact on the overlap integrals between signal mode profiles and the erbium dopant distribution and thus the DMG performance. Several designs and analyses have been reported recently aimed at reducing the DMG of RCF-based EDFAs.
Pumping configuration: Compared with core pumping, cladding pumping has advantages in lower DMG for RCF-EDFAs, even when considering fibre impairments (e.g. micro-bending of fibre, etc.). Q. Kang *et al.* analysed overlap integrals between the mode intensity profiles and the erbium dopant distribution of a GI-RCF EDFA at fibre bending radius of 5cm [77]. Their simulation results show that the overlap integrals between the mode intensity profile and erbium dopant profile is significantly decreased for the low-order modes (e.g. the LP_{01}, LP_{11} modes) at such bending radius, compared to when the fibre is relatively straight. As a result, the DMG under such bending showed significant dependence on the pump mode selected under the core-pumped condition, while cladding-pumping showed higher tolerance to the micro-bending [77]. They also evaluated the performance of the air-core EDFA under both core-pumped and cladding-pumped operations [78], and the DMG of the former case was also found to depend on the pump

mode used significantly while the pump-mode dependency of DMG in the latter case could be almost neglected. The larger DMG of the air-core EDFA under core-pumped operation mainly resulted from differences in the overlap of the pump modes, signal modes and the distribution of the rare-earth dopant in the SI-RCF with large differential RI between the core and the inner air cladding [78]. Although cladding pumping exhibits better DMG performance, double-clad fibre architecture and relatively higher coupling loss of the pump mode power should be considered in the practical implementations [75, 78].

Erbium doping profile: optimized erbium doping profile will help decrease the pump-mode dependency of DMG for core-pumped RCF-EDFAs. In [78], Q. Kang *et al.* pointed out that confined doping profile could relieve the pump mode dependency for core pumped operation. In [79], M. Yamada *et al.* reported that larger parameter α for the α-th power profile and smaller parameter x for the trapezoid profile of the erbium doping distribution could help to reduce the DMG of their 2-LP-mode RCF-EDFA under core-pumped condition. A. Gaur *et al.* also reported that extra annulus doping helped in reducing DMG of higher-order MGs in their design of RCF-based EDFA [80].

RI profiles of the RCFs: The RI profile will also affect the DMG performance of the core-pumped RCF-EDFAs. H. Ono *et al.* analysed how the combinations of the inner and outer radius of the SI-RCF affected the DMG of their 2-LP-mode RCF-based EDFAs and reported that low DMG could be achieved by adopting the inner radius of about 2.5–4 μm and the outer radius near the LP_{21} cut-off values [81, 82]. Based on simulation [77] and experimental [76] results, Y. Jung *et al.* showed that lower DMG of the EDFA could be achieved by utilizing GI-RCF under core-pumped operation without severe micro-bending, compared with that of the SI-RCF EDFA with large differential RI between core and cladding [78].

If the RCF-EDFA is to be adapted for further up-scaled MDM communications systems, a fundamental constraint to the RI profile is that it must support at least the same number of MGs as the transmission fibre. This would require simultaneous high Δn doping and elaborate Er doping profiles, which is likely to challenge existing EDFA fabrication technologies.

B. RCF Raman Amplifiers

According to the theoretical analysis in [83], the DMG of the Raman amplification in MMFs is strongly dependent on the intensity overlap integrals between different spatial modes, which can be expressed as:

$$f_{n,m} = \frac{\iint\limits_{-\infty}^{+\infty} I_n(x, y) I_m(x, y) dxdy}{\iint\limits_{-\infty}^{+\infty} I_n(x, y) dxdy \iint\limits_{-\infty}^{+\infty} I_m(x, y) dxdy} \qquad (12)$$

where $I_n(x, y)$ and $I_m(x, y)$ represents the intensity distributions of the n_{th} and m_{th} spatial modes (one being the pump mode and the other being the signal mode) in the fibre cross section, respectively. Here the wavelength dependence of the mode profile is assumed to be negligible. As shown in Table I, very similar overlap integrals can be achieved in the RCFs due to the

radial confinement within the ring core, which can be confirmed by the calculation results according to Eq.12 base on the GI-RCF that we reported in [39, 45]. These results indicate that very good DMG performance could be achieved by pumping in a MG that has the least variance in terms of its overlap integral with other modes, e.g., the $|l|$=3 or 4 MG.

TABLE I
INTENSITY OVERLAP INTEGRALS (IN $10^9/ M^2$) BETWEEN MODE GROUPS OF THE GI-RCF

		$|l|$=0	$|l|$=1	$|l|$=2	$|l|$=3	$|l|$=4	$|l|$=5	Standard Deviation
				Pump mode @ 1455nm				
Signal mode @ 1560nm	$|l|$=0	7.97	7.97	7.95	7.91	7.82	7.62	0.14
	$|l|$=1	7.97	7.97	7.96	7.92	7.84	7.65	0.13
	$|l|$=2	7.95	7.96	7.95	7.94	7.88	7.72	0.09
	$|l|$=3	7.91	7.92	7.94	7.96	7.94	7.82	0.05
	$|l|$=4	7.82	7.84	7.88	7.94	7.96	7.89	0.05
	$|l|$=5	7.62	7.65	7.72	7.81	7.89	7.90	0.12

L. Zhu *et al.* [24] experimentally demonstrated the first OAM distributed Raman amplifier using the 18-km GI-RCF designed by our research group [28], achieving an on-off gain of between 2.5 – 3.5 dB, as shown in Fig.10, with very low DMG of < 0.5 dB between the two high-order OAM modes over the C band. The reported Raman gain is still quite limited, mainly due to the slightly high attenuation of the fibre (0.75 dB/km), limiting the nonlinear effective length to ~5.7 km. Another feature of the RCF, namely its large effective mode area, which is beneficial to the transmission of high number of signal channels (including MDM and WDM) with low nonlinear crosstalk, is counter-productive to Raman gain. Further studies of RCF-based Raman amplifiers would be reported in future, whose performances are likely to be enhanced due to reduced fibre attenuation and better pump-beam coupling.
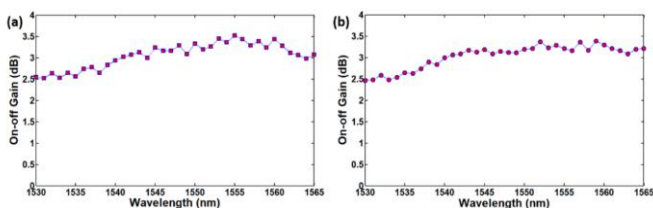

Fig. 10. Measure on-off gain of (a) OAM+4 and (b) OAM+5 modes in the RCF-based Raman amplifiers [24].

VI. DATA TRANSMISSION OF RCF-BASED MDM SYSTEMS

Recently reported RCF-based MDM communication experiments fall into two categories according to whether MIMO equalization was needed.

A. MIMO-free MDM system over RCFs

Considering that short-reach transmission systems are sensitive to cost and power consumption, MIMO-free intensity-modulation direct-detection (IM-DD) schemes are often considered more favourable [84]. Such schemes have been implemented using cylindrical RCF-based OAM-MDM, MGM, and also elliptical RCF-based MDM schemes.

N. Bozinovic *et al.* demonstrated the first OAM-MDM fibre transmission with four OAM modes up to the order $|l|$ = 1 [30]. The high-index ring RI profile of the 'vortex fibre' used broke the quasi-degeneracy between the desired $OAM^{\pm}$ and parasitic TM_{01} and TE_{01} modes, hence minimizing modal crosstalk between them and decreasing the MIMO complexity. Successful transmission of 400-Gb/s data at a single wavelength and 1.6-Tb/s data at 10 wavelengths over 1.1-km fibre was achieved.

Based on the inverse-parabolic graded-index fibre (IPGIF) with a modal index separation $\Delta n_{eff} > 2.1\times10^{-4}$ between non-degenerate modes within the same MG (e.g. the left- circularly polarized OAM_{+2} and OAM_{-2} modes), X. Wang *et al.* demonstrated 3.36-Tbit/s transmission of 28-Gbaud QPSK signals over a 100-m IPGIF, with 15 wavelength channels each multiplexed 4 OAM modes up to the order $|l|$ = 2. Only 2×2 MIMO processing or optical polarization controllers were required to mitigate the crosstalk between the degenerate modes of the same spin-orbital alignment (e.g. the right-circularly polarized OAM_{+2} and left-circularly polarized OAM_{-2} modes) [85].

As mentioned in Section I, in the cylindrical RCF MGM scheme, the strongly-coupled intra-MG modes are considered as one data channel and weak inter-MG coupling can be used to eliminate MIMO. Two major problems can be encountered in MGM schemes, namely mode partition noise (MPN) at the receiver and frequency selective fading resulting from intra-MG DMD [86]. MPN can be dealt with by simultaneously detecting all the intra-group modes [19, 20], but the fading resulting from the intra-group DMD cannot be eliminated by schemes such as single-side band modulation [84,28] which would be effective in dealing with fading in SMF due to chromatic dispersion.

F. Feng *et al.* demonstrated all-optical MGM transmission experiments, carrying 10Gb/s OOK signals on 2 LP MGs over 24-km GI-RCF and 3 LP MGs over 360-m GI-RCF, respectively [40, 87-89]. In these experiments, simultaneous detection of all the intra-MG modes was realized using weighted composite phase masks to avoid the mode partition noise. The low intra-MG DMD of the RCF used also helped reduce fading of the received signals. The authors [28] demonstrated an OAM-MGM scheme using phase-plate based OAM demultiplexer and receive-diversity techniques, in which a maximal-ratio-combining algorithm was employed to adaptively suppress the MPN and improve the signal-to-noise ratio (SNR) of the received signals, as shown in Fig. 11 [28]. The low RI gradient GI-RCF (as described earlier) provided very low intra-MG DMD which relieved the frequency-selective fading in the directly-detected signals. 3-MG 100-Gb/s and 2-MG multiplexed 40-Gb/s discrete multi-tone (DMT) signals were respectively transmitted over 1-km and 18.4-km GI-RCF successfully. More recently, 8.4-Tbit/s MIMO-free data transmission over the same 18-km GI-RCF has been demonstrated successfully, in which two OAM modes (OAM_{+4} and OAM_{-5}) with 112 WDM channels are multiplexed to give 224 data channels, with each channel carrying a 12.5-Gbaud 8-QAM signal [90-91]
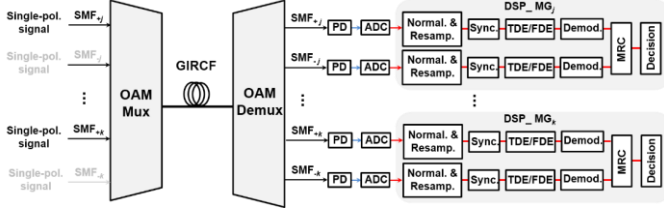
Fig. 11. Block diagram of the OAM mode-group (de)multiplexing scheme. SMF_i: the single mode fibre input/output port for the i_{th} OAM mode; MG_i: the i_{th} OAM mode group including OAM modes $<\pm i, \pm s>$ ($i \in \{j, j+1, \ldots, k\}$ in which k and j are integers, and $k > j > 0$; $\pm i$ being the azimuthal mode order and $\pm s$ being the left- or right-hand circular polarizations); Normal.: Normalization; Resamp.: resampling; demod.: demodulation [28].

Based on the polarization maintaining elliptical RCF mentioned in Section III, L. Wang *et al.* demonstrated a MIMO-free QPSK transmission system over 0.9 km using six LP vector modes as independent data channels. Low crosstalk during fibre transmission is achieved among the six LP vector modes with Δn_{eff} larger than 1×10^{-4} [92, 93]. R. M. Nejad *et al.* also demonstrated a MDM radio over fibre (RoF) transmission experiment over a 0.9-km polarization maintaining elliptical RCF using four LP vector modes, achieving successful transmission of 4×1.152-Gb/s 16QAM–OFDM signals [94].

B. RCF-Based MDM Systems with modular MIMO

As proposed in Section II, in order to further improve the system capacity per wavelength (or SE), RCF-based MDM systems with coherent detection and MIMO equalisation could be used [95].

Based on a SI-RCF [37] and mode selective RCF PLs [70], K. Shi *et al.* demonstrated a MDM transmission system supporting 5 spatial modes, transmitting raw data rate of 1.12 Tb/s/λ over 1 km and 560Gb/s/λ over 24 km of RCF, using Nyquist dual-polarization 16QAM and QPSK signals, respectively [71]. However, full 10x10 MIMO processing was required in this system mainly because of the high modal crosstalk in the PLs as mode MUX/DEMUX as well as the relatively high coupling between the MGs of LP_{01} and $LP_{11a/b}$ resulted from their small Δn_{eff}.

In order to demonstrate the more scalable modular 4x4 MIMO scheme (as shown in Fig. 12) as described in Section II, the authors implemented an MDM transmission experiment over a 10-km GI-RCF utilizing 8 OAM modes belonging to MG-4 and MG-5 that are de-coupled by the large inter-MG Δn_{eff} [39]. 10 wavelengths channels each modulated by 32 GBaud QPSK are transmitted over the 8 MDM channels, achieving a total capacity of 5.12 Tb/s and a spectral efficiency of 16 bits/s/Hz. The MIMO complexity is not only limited in its scale at 4x4, but also further alleviated by the very low intra-MG DMD afforded by the specially designing low RI gradient GI-RCF, which resulted in only 15 taps being needed.
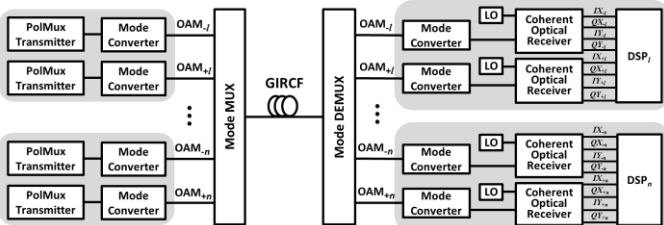

Fig. 12. Block diagram of the RCF-based OAM MDM digital coherent transceiver system. LO: local oscillator; DSP_i: digital signal processing module for the i_{th} OAM mode group including OAM modes $< \pm i, \pm s>$ ($i = l, \ldots n$, in which $l > 1$; $\pm i$ being the azimuthal mode order and $\pm s$ being the left- or right-hand circular polarizations) [39].

VII. CONCLUSIONS AND DISCUSSIONS

In this paper, we have reviewed key aspects of RCF-based MDM optical fibre transmission.

We first present a theoretical study on its potentials for low signal processing complexity compared with MDM schemes based on SI- and GI-MMFs. Our simulation results show that among the three MDM schemes in the comparison, RCF-MDM would exhibit the lowest signal processing complexity in achieving the same spectral efficiency due to its potential ability to support mode-group based fixed-size modular MIMO or MIMO-free transmission.

We then reviewed various RCFs designed aiming at supporting MIMO-free and modular MIMO transmission schemes, delimited by four key design parameters of ring-core radius R, ring width W, core-cladding Δn, and RI profile. A detailed discussion on the role of the radial RI gradient has been given - while high RI gradient can be exploited to split modes in the same MG for OAM transmission with 2x2 MIMO or even without MIMO equalization, low RI gradient is shown to produce low intra-MG DMD that enables lower MIMO complexity MDM transmission and good channel response for MIMO-free MGM transmission. A discussion on the RCF's potentials for providing high mode channel count under various inter-MG Δn_{eff} criteria for short-, medium-, and long-distance transmission has been presented, which shows that RCFs can theoretically support tens of MDM channels depending on the transmission distance. We also discussed how the RCF RI profile could be engineered for even lower inter-MG coupling by extending the fibre perturbation model to higher order Taylor analysis.

Device schemes for (de-)multiplexing of RCF modes have been reviewed. It is believed that unitary optical transformation devices should provide more scalable solutions, provided they overcome problems in mode matching. Fibre-based devices have low insertion loss and could also enable scalable wideband MUX/DEMUX solutions, however need to overcome crosstalk issues as channel number increases, while PIC-based schemes need to overcome insertion loss issues and other scheme-specific issues such as optical bandwidth and polarization matching.

RCF-based optical amplifiers (both rare-earth doped and Raman) are shown to deliver low differential mode gain due to the radial confinement of light in the ring core. Recently-reported RCF-based EDFAs and Raman amplifiers as well as the efforts on optimization of their DMG performance have been reviewed for further improvement of system power budget and increase of transmission distance.

RCF-MDM data transmission experiments, including MIMO-free OAM, MIMO-free MGM, and modular MIMO MDM schemes have been summarized. Generally, these have demonstrated potentials for short-reach data transmission, with the maximum single-span transmission distance reaching ~ 24 km. Longer-distance RCF-MDM data transmissions are

believed to be realisable in the future, on the basis of further optimised fibre, MUX/DEMUX, amplification, and DSP algorithms according to the RCF channel characteristics.

Despite its potentials and the progress made in the reviewed research activities, RCF MDM transmission technology still faces significant challenges in long-haul oriented transmission, in that capacity-distance product or SE-distance product comparable to those demonstrated in MCFs or FMF has not yet been demonstrated, primarily because the transmission distance has been limited by both attenuation and crosstalk. This limitation needs to be broken by implementing RCF fibre loop testbed that integrates high quality ring-core transmission fibre (with very low inter-mode or inter-MG crosstalk at the levels of < -20 dB/100-km) and RCF amplifiers - such looped have been demonstrated for FMF and MCFs with transmission distances in the 10^{3-4} km range. On the other hand, for distances of up to ~ 20 km, inter-mode or inter-MG crosstalk levels in the order or -10 to -20 dB have enabled a rich variety of RCF-based short-reach transmission experiments, and research efforts in this respect would be best directed toward demonstrating very high mode channel count transmission of various data formats that require very low complexity DSP.

REFERENCES

[1] D. J. Richardson, J. M. Fini, and L. E. Nelson, "Space-division multiplexing in optical fibres," Nat. Photonics 7, 354 (2013).

[2] G. Li, N. Bai, N. Zhao, and C. Xia, "Space-division multiplexing: the next frontier in optical communication," Adv. Opt. Photonics 6, 413 (2014).

[3] S. Randel, R. Ryf, A. Sierra, P. J. Winzer, A. H. Gnauck, C. A. Bolle, R. J. Essiambre, D. W. Peckham, A. McCurdy, and R. Lingle, "6× 56-Gb/s mode-division multiplexed transmission over 33-km few-mode fiber enabled by 6× 6 MIMO equalization," Opt. Express 19(17), 16697–16707 (2011).

[4] S. O. Arik, K.-P. Ho, and J. M. Kahn, "Optical network scaling: roles of spectral and spatial aggregation," Opt. Express 22(24), 29868–29887 (2014).

[5] P. J. Winzer, "Making spatial multiplexing a reality," Nat. Photonics 8, 345–348 (2014).

[6] S. O. Arik, D. Askarov, and J. M. Kahn, "Effect of mode coupling on signal processing complexity in mode-division multiplexing," J. Lightwave Technol. 31(3), 423–431 (2013).

[7] S. O. Arik, K.-P. Ho, and J. M. Kahn, "Group Delay Management and Multiinput Multioutput Signal Processing in Mode-Division Multiplexing Systems," J. Lightwave Technol. 34(11), 2867–2880 (2016).

[8] K.-P. Ho and J. M. Kahn, "Statistics of group delays in multimode fiber with strong mode coupling," J. Lightwave Technol. 29(21), 3119–3128 (2011).

[9] R. Murayama, N. Kuwaki, S. Matsuo, and M. Ohashi, "Relationship between mode coupling and fiber characteristics in few-mode fibers analyzed using impulse response measurement technique," J. Lightwave Technol. 35, 650 (2017).

[10] C. Koebele et al., "40km Transmission of Five Mode Division Multiplexed Data Streams at 100Gb/s with Low MIMO-DSP Complexity," Proc. ECOC, Th.13.C.3. (2011).

[11] Daiki Soma, Yuta Wakayama, Koji Igarashi, and Takehiro Tsuritani, "Partial MIMO-based 10-Mode-Multiplexed Transmission over 81km Weakly-coupled Few-mode Fiber," Proc. OFC, M2D.4 (2017).

[12] Ge, Dawei, et al. "Design of a Weakly-Coupled Ring-Core FMF and Demonstration of 6-mode 10-km IM/DD Transmission." Optical Fiber Communication Conference. Optical Society of America, 2018.

[13] E. Ip, G. Milione, M. J. Li, N. Cvijetic, K. Kanonakis, J. Stone, G. Peng, X. Prieto, C. Montero, V. Moreno, and J. Liñares, "SDM transmission of real-time 10GbE traffic using commercial SFP + transceivers over 0.5km elliptical-core few-mode fiber," Opt. Express 23(13), 17120–17126 (2015).

[14] G. Milione et al., "MIMO-less space division multiplexing with elliptical core optical fibers," Proc. OFC, Tu2J.1 (2017).

[15] L. Wang et al., "MDM transmission of CAP-16 signals over 1.1-km anti-bending trench-assisted elliptical-core few-mode fiber in passive optical networks," Optics express, 25(19), 22991-23002 (2017).

[16] Y. H. Kim and K. Y. Song,"Mapping of intermodal beat length distribution in an elliptical-core two-mode fiber based on Brillouin dynamic grating," Opt. Express22, 17292–17302 (2014).

[17] B. Franz, and H. Bülow, "Mode Group Division Multiplexing in Graded‐Index Multimode Fibers," Bell Labs Technical Journal 18, 153–172 (2013).

[18] H. Liu, H. Wen, J. C. A. Zacarias, J. Antonio-Lopez, N. Wang, P. Sillard, A. Amezcua-Correa, R. A. Correa, and G. Li, "3x10 Gb/s mode group-multiplexed transmission over a 20 km few-mode fiber using photonic lanterns," in Optical Fiber Communication Conference, OSA Technical Digest (online) (Optical Society of America, 2017), paper M2D.5.

[19] G. Labroille, P. Jian, L. Garcia, J.-B. Trinel, R. Kassi, L. Bigot, J.-F. Morizur , "30 Gbit/s Transmission over 1 km of Conventional Multimode Fiber using Mode Group Multiplexing with OOK modulation and direct detection," in Optical Communication (ECOC), 2015 European Conference on IEEE 2015, pp. 1–3.

[20] K. Benyahya, C. Simonneau, A. Ghazisaeidi, N. Barré, P. Jian, J. Morizur, G. Labroille, M. Bigot, P. Sillard, J. G. Provost, H. Debrégeas, J. Renaudier, and G. Charlet, "Multiterabit Transmission over OM2 Multimode Fiber with Wavelength and Mode Group Multiplexing and Direct Detection," Journal of Lightwave Technology, 36(2): 355-360(2018).

[21] D. Gloge and E. A. J. Marcatili, "Impulse Response of Fibers with Ring-Shaped Parabolic Index Distribution", Bell Labs Tech. J. 52, 1161 (1973).

[22] X. Jin et al., "Mode Coupling Effects in Ring-Core Fibers for Space-Division Multiplexing Systems," J. Lightwave Technol. 34, 3365 (2016).

[23] Q. Kang, E. Lim, Y. Jun, X. Jin, F. P. Payne, S. Alam, and D. J. Richardson, "Gain Equalization of a Six-Mode-Group Ring Core Multimode EDFA," in Optical Communication (ECOC), 2014 European Conference on IEEE 2014 pp. 1–3.

[24] L. Zhu, J. Li, G. Zhu, L. Wang, C. Cai, A. Wang, S. Li, M. Tang, Z. He, S. Yu, C. Du, W. Luo, J. Liu, J. Du, J. Wang, "First Demonstration of Orbital Angular Momentum (OAM) Distributed Raman Amplifier over 18-km OAM Fiber with Data-Carrying OAM Multiplexing and Wavelength-Division Multiplexing," in Optical Fiber Communication Conference (Optical Society of America, 2018), paper W4C.4.

[25] D. Gloge, "Weakly Guiding Fibers," Appl. Opt. 10, 2252 (1971).

[26] G. Keiser, Optical fiber communications, 3rd ed. Pearson Education Limited, 2003.

[27] D. Marcuse, "Microdeformation losses of single-mode fibers," Appl. Opt. 23, 1082 (1984).

[28] J. Zhang, G. Zhu, J. Liu, X. Wu, J. Zhu, C. Du, W. Luo, Y. Chen, and S. Yu, "Orbital-angular-momentum mode-group multiplexed transmission over a graded-index ring-core fiber based on receive diversity and maximal ratio combining," Opt. Express 26(4), 4243–4257 (2018).

[29] Allen, Les, et al. "Orbital angular momentum of light and the transformation of Laguerre-Gaussian laser modes." Physical Review A 45.11 (1992): 8185.

[30] N. Bozinovic, Y. Yue, Y. Ren, M. Tur, P. Kristensen, H. Huang, A. E. Willner, and S. Ramachandran, "Terabit-scale orbital angular momentum mode division multiplexing in fibers," Science 340, 1545 (2013).

[31] B. Vucetic and J. Yuan, Space-Time Coding. 2003.

[32] N. Savage, "Information theory after Shannon," Commun. ACM, vol. 54, no. 2, p. 16, 2011.

[33] T. M. Cover and J. A. Thomas, Elements of Information Theory. 2005.

[34] Zhao, Ningbo, et al. "Capacity limits of spatially multiplexed free-space communication." Nature photonics 9.12 (2015): 822.

[35] R. M. Nejad, K. Allahverdyan, P. Vaity, S. Amiralizadeh, C. Brunet, and Y. Messaddeq, et al. "Orbital angular momentum mode division multiplexing over 1.4 km RCF fiber," Lasers and Electro-Optics (pp.SW4F.3). IEEE. (2016).

[36] S. Ramachandran, P. Kristensen, and M. F. Yan. "Generation and propagation of radially polarized beams in optical fibers." Optics Letters 34, 2525 (2009)

[37] B. Ung, C. Brunet, L. A. Rusch, L. Wang, S. Larochelle, and Y. Messaddeq, "Design of a family of ring-core fibers for oam transmission studies," Optics Express 23, 10553 (2015).

[38] S. Ramachandran, "Optical vortices in fiber," Nanophotonics 2, 455 (2013).

[39] G. Zhu, Z. Hu, X. Wu, C. Du, W. Luo, and Y. Chen, et al. (2018). Scalable mode division multiplexed transmission over a 10-km ring-core fiber using high-order orbital angular momentum modes. Optics Express, 26(2), 594-604.

[40] F. Feng, X. Guo, G. S. D. Gordon, X. Q. Jin, F. P. Payne, and Y. Jung, et al. "All-optical mode-group division multiplexing over a graded-index ring-core fiber with single radial mode," Optical Fiber Communications Conference and Exhibition (Vol.25, pp.13773). IEEE. (2016).

[41] C. Brunet, and L. A. Rusch, "Optical fibers for the transmission of orbital angular momentum modes," Optical Fiber Technology 35, (2017).

[42] A. Rubano, F. Bao, F. D. Ros, H. Hu, K. K. Rottwitt, and K. Ingerslev, et al. "12 Mode, MIMO-Free OAM Transmission," Optical Fiber Communications Conference and Exhibition (pp.M2D.1). IEEE. (2017).

[43] P. Gregg, P. Kristensen, and S. Ramachandran, "Conservation of orbital angular momentum in air-core optical fibers," Physics 2, 267 (2015)

[44] Jung, Yongmin, et al. "Low-Loss 25.3 km Few-Mode Ring-Core Fiber for Mode-Division Multiplexed Transmission." Journal of Lightwave Technology 35.8 (2017): 1363-1368.

[45] G. Zhu, J. Zhu, X. Wu, J. Liu, C. Du, H. Yan, Z. Hu, X. Wang, Y. Chen, W. Luo, S. Li, X. Zheng, X. Cai, and S. Yu, "Scalable Orbital Angular Momentum Mode Division Multiplexing Transmission over 10km Graded-index Ring-core Fiber," in 2017 IEEE European Conference on Optical Communication (IEEE 2017), pp. 1–3

[46] P. Gregg, P. Kristensen, S. Ramachandran, and S. E. Golowich, "On the scalability of ring fiber designs for oam multiplexing," Optics Express 23, 3721 (2015).

[47] L. Wang and S. LaRochelle, "Design of eight-mode polarization-maintaining few-mode fiber for multiple-input multiple-output-free spatial division multiplexing," Opt. Lett.40, 5846–5849(2015).

[48] J. Zhao et al., "Polarization-maintaining few mode fiber composed of a central circular-hole and an elliptical-ring core," Photonics Research, 2017, 5(3): 261-266.

[49] H. Yan, S. Li, Z. Xie, X. Zheng, H. Zhang, and B. Zhou, "Design of PANDA ring-core fiber with 10 polarization-maintaining modes," Photonics Research, 5(1), 1-5(2017).

[50] Cao, Yuan, et al. "Design of 16-mode PANDA polarization-maintaining ring-core fiber for MIMO-free space-division multiplexing." Optical Communications and Networks (ICOCN), 2017 16th International Conference on. IEEE, 2017.

[51] J. Leach, M. J. Padgett, S. M. Barnett, S. Frankearnold , and J. Courtial, "Measuring the orbital angular momentum of a single photon," Phys. Rev. Lett. vol. 88, no. 25, pp. 257901, 2002.

[52] E. Karimi, B. Piccirillo, E. Nagali, L. Marrucci, and E. Santamato, "Efficient generation and sorting of orbital angular momentum eigenmodes of light by thermally tuned qq-plates," Appl. Phys. Lett., vol. 94, no. 23, pp. 231124, 2009.

[53] J.-F. Morizur, L. Nicholls, P. Jian, S. Armstrong, N. Treps, B. Hage, M. Hsu, W. Bowen, J. Janousek, and H.-A. Bachor, "Programmable unitary spatial mode manipulation," J. Opt. Soc. Am. A vol. 27, no. 11, pp. 2524–2531, 2010.

[54] G. Labroille, B. Denolle, P. Jian, P. Genevaux, N. Treps, and Jean-Francois Morizur, "Efficient and mode selective spatial mode multiplexer based on multi-plane light conversion," Opt. Express, vol. 22, no. 13, pp. 15599-15607, 2014.

[55] G. Labroille, P. Jian, N. Barre, B. Denolle, J. Morizur, "Mode Selective 10-Mode Multiplexer based on Multi-Plane Light Conversion," in Optical Fiber Communication (OFC) Conference, 2016, p. Th3E.5.

[56] G. C. G. Berkhout, M. P. J. Lavery, J. Courtial, M. W. Beijersbergen, and M. J. Padgett, "Efficient sorting of orbital angular momentum states of light," Phys. Rev. Lett., vol. 105, no. 153601, pp. 153601, 2010.

[57] Y. Wen, I. Chremmos, Y. Chen, J. Zhu, Y. Zhang, and S. Yu, "Spiral Transformation for High-Resolution and Efficient Sorting of Optical Vortex Modes," Phys. Rev. Lett., 2018, accepted for publication.

[58] C. R. Doerr, N. K. Fontaine, M. Hirano, T. Sasaki, L. L. Buhl, and P. J. Winzer, "Silicon photonic integrated circuit for coupling to a ring-core multimode fiber for space-division multiplexing," in European Conference on Optical Communication (ECOC), 2011, p. Th.13.A.3.

[59] T. Su, R. P. Scott, S. S. Djordjevic, N. K. Fontaine, D. J. Geisler, X. Cai, and S. J. B. Yoo, "Demonstration of free space coherent optical communication using integrated silicon photonic orbital angular momentum devices," Opt. Express, vol. 20, no. 9, pp. 9396-9402, 2012.

[60] B. Guan, R. P. Scott, C. Qin, N. K. Fontaine, T. Su, C. Ferrari, M. Cappuzzo, F. Klemens, B. Keller, M. Earnshaw, and S. J. B. Yoo, "Free-space coherent optical communication with orbital angular, momentum multiplexing/demultiplexing using a hybrid 3D photonic integrated circuit," Opt. Express, vol. 22, no. 1, pp. 145-156, 2013.

[61] X. Cai, J. Wang, M. J. Strain, B. Johnson-Morris, J. Zhu, Marc Sorel, J. L. O'Brien, M. G. Thompson, S. Yu, "Integrated compact optical vortex beam emitters," Science, vol. 338, no. 6105, pp. 363-366, 2012.

[62] S. Li, Z. Nong, S. Gao, M. He, L. Liu, S. Yu, X. Cai, "Orbital Angular Momentum Mode Multiplexer Based on Bilayer Concentric Micro-Ring Resonator," in Asia Communications and Photonics Conference (ACP), 2017, p. Su3K.2.

[63] N. Zhang, M. Scaffardi, M. N. Malik, V. Toccafondo, C. Klitis, G. Meloni, F. Fresi, E. Lazzeri, D. Marini, J. Zhu, X. Cai, S. Yu, L. Poti, A. Bogoni, and M. Sorel, "4 OAM x 4 WDM Optical Switching Based on an Innovative Integrated Tunable OAM Multiplexer," in Optical Fiber Communication (OFC) Conference, 2018, p. Th3H.1.

[64] Shao, Zengkai, et al. "Spin-orbit interaction of light induced by transverse spin angular momentum engineering." Nature communications 9.1 (2018): 926.

[65] Y. Chen, L. A. Rusch, and W. Shi, "Integrated Circularly Polarized OAM Generator and Multiplexer for Fiber Transmission," IEEE Journal of Quantum Electronics, vol. 54, no. 2, pp. 8400109, 2018.

[66] Chen, Haoshuo, et al. "Compact spatial multiplexers for mode division multiplexing." Optics express 22.26 (2014): 31582-31594.

[67] Y. Yan, Y. Yue, H. Huang, J. Yang, M. R. Chitgarha, N. Ahmed, M. Tur, S. J. Dolinar, and A. E. Willner, "Efficient generation and multiplexing of optical orbital angular momentum modes in a ring fiber by using multiple coherent inputs," Opt. Lett., vol. 37, no.17, pp. 3645-3647, 2012.

[68] S. Pidishety, S. Pachava, P. Gregg, S. Ramachandran, G. Brambilla, and B. Srinivasan, "Orbital angular momentum beam excitation using an all-fiber weakly fused mode selective coupler," Opt. Lett., vol. 42, no. 21, pp. 4347-4350, 2017.

[69] T. A. Birks, I. Gris-Sánchez, S. Yerolatsitis, S. G. Leon-Saval, and R. R. Thomson, "The photonic lantern," Adv. Opt. Photon., vol. 7, no.2, pp. 107-167, 2015.

[70] Z. S. Eznaveh, J. C. A. Zacarias, J. E. A. Lopez, Y. Jung, K. Shi, B. C. Thomsen, D. J. Richardson, S. Leon-Saval, and R. A. Correa, "Annular Core Photonic Lantern OAM Mode Multiplexer," in Optical Fiber Communication (OFC) Conference, 2017, p. Tu3J.3.

[71] K. Shi, Y. Jung, Z. S. Eznaveh, J. C. A. Zacarias, J. E. A. Lopez, H. Zhou, R. Zhang, S. Chen, H. Wang, Y. Yang, R. A. Correa, D. J. Richardson, and B. C. Thomsen, "10×10 MDM Transmission over 24 km of Ring-Core Fibre using Mode Selective Photonic Lanterns and Sparse Equalization," in European Conference on Optical Communication (ECOC), 2017, p. M.2.E.2.

[72] J. Zhou, "OAM states generation/detection based on the multimode interference effect in a ring core fiber," Opt. Express, vol. 23, no. 8, pp. 10247-10258, 2015.

[73] H. Ono, T. Hosokawa, K. Ichii, S. Matsuo and M. Yamada, "Improvement of differential modal gain in few-mode fibre amplifier by employing ring-core erbium-doped fibre," Electronics Letters 51(2), 172-173 (2015).

[74] Y. Amma , T. Hosokawa, H. Ono , K, Ichii, K. Takenaga, S. Matsuo, and M. Yamada, "Ring-Core Multicore Few-Mode Erbium-Doped Fiber Amplifier," IEEE PHOTONICS TECHNOLOGY LETTERS, 29(24), 2163-2166 (2017)

[75] Y. Jung et al., "Optical orbital angular momentum amplifier based on an air-core erbium doped fiber," inProc. Opt. Fiber Commun. Conf. Post-deadline Papers, 2016, Paper Th5A.5

[76] Y. Jung et al., "Few mode ring-core fiber amplifier for low differential modal gain." (2017).

[77] Q. Kanget al., "Gain equalization of a six-mode group ring core multimode EDFA," in Proc. 40th Eur. Conf. Exhib. Opt. Commun., 2014, Paper P.1.14.

[78] Q. Kang et al., "Amplification of 12 OAM modes in an air-core erbium doped fiber," Opt. Express, vol. 23, pp. 28341–28348, 2015.

[79] M. Yamada, D. Nobuhira, S. Miyagawa, O. Koyama, and H. Ono, "Doping concentration distribution in 2-signal LP-mode ring-core erbium-doped fiber," Applied Optics, 56(36), 10040-10045, (2017).

[80] A. Gaur and V. Rastogi, "Design and Analysis of Annulus Core Few Mode EDFA for Modal Gain Equalization," IEEE PHOTONICS TECHNOLOGYLETTERS, 28(10), 2016

[81] H. Ono, T. Hosokawa, K. Ichii, S. Matsuo, H. Nasu, and M. Yamada, "2-LP mode few-mode fiber amplifier employing ring-core erbium-doped fiber," Optics Express, 23(21), 27405-27418, (2015).

[82] S. Miyagawa, D. Nobuhir, O. Koyama, M. Yamada, and H. Ono, "Study on structural parameters of 2-LP mode ring-core erbium-doped fiber," In Opto-Electronics and Communications Conference (OECC) and Photonics Global Conference (PGC), 2017 (pp. 1-2). IEEE.

[83] R. Ryf, R. Essiambre, J. von Hoyningen-Huene, and P. Winzer, "Analysis of mode-dependent gain in Raman amplified few-mode fiber," in Optical Fiber Communication Conference, OSA Tech. Digest (Optical Society of America, 2012), paper OW1D.2.

[84] K. Zhong, X. Zhou, J. Huo, C. Yu, C. Lu, and A. P. T. Lau, "Digital Signal Processing for Short-Reach Optical Communications: A Review of Current Technologies and Future Trends," Journal of Lightwave Technology, 36(2), 377-400(2018).

[85] X. Wang et al., "3.36-Tbit/s OAM and wavelength multiplexed transmission over an inverse-parabolic graded index fiber." Lasers and Electro-Optics (CLEO), 2017 Conference on. IEEE, 2017.

[86] Yong Soo Cho, Jaekwon Kim, Won Young Yang, Chung-Gu Kang,MIMO-OFDM Wireless Communication with MATLAB, John Wiley &Sons (Asia), Singapore, 2010.

[87] F. Feng, Y. Jung, H. Zhou, R. Zhang, S. Chen, H. Wang, Y. Yang, S. U. Alam, D. J. Richardson, and Timothy D. Wilkinson, "High-Order Mode-Group Multiplexed Transmission over a 24km Ring-Core Fibre with OOK Modulation and Direct Detection," in Optical Communication (ECOC), 2017 European Conference on IEEE 2017, pp. 1–3.

[88] F. Feng, X. Jin, D. O'Brien, F. P. Payne, and T. D. Wilkinson, "Mode-Group Multiplexed Transmission using OAM modes over 1 km Ring-Core Fiber without MIMO Processing," in Optical Fiber Communication Conference (Optical Society of America, 2017), paper Th2A.43.

[89] Feng, Feng, et al. "All-optical mode-group multiplexed transmission over a graded-index ring-core fiber with single radial mode." Optics Express 25.12 (2017): 13773-13781.

[90] Zhu, Long, et al. "18 km low-crosstalk OAM+ WDM transmission with 224 individual channels enabled by a ring-core fiber with large high-order mode group separation." Optics letters 43.8 (2018): 1890-1893.

[91] Zhu, Long, et al. "Experimental Demonstration of 8.4-Tbit/s Data Transmission over an 18-km Orbital Angular Momentum (OAM) Fiber using WDM and OAM based Mode Division Multiplexing (MDM)." Optical Communication (ECOC), 2017 European Conference on. IEEE, 2017.

[92] Wang, Lixian, et al. "Linearly polarized vector modes: enabling MIMO-free mode-division multiplexing." Optics express 25.10 (2017): 11736-11749.

[93] Wang, Lixian, et al. "MIMO-free transmission over six vector modes in a polarization maintaining elliptical ring core fiber." Optical Fiber Communications Conference and Exhibition (OFC), 2017. IEEE, 2017.

[94] Nejad, Reza Mirzaei, et al. "Four-Channel RoF Transmission over Polarization Maintaining Elliptical Ring Core Fiber." Optical Fiber Communication Conference. Optical Society of America, 2018.

[95] Y. Sone, et al., "Systems and technologies for high speed inter-office/datacenter Interface," in Proc. of SPIE Vol. 2017, 10131: 101310D-10.